# **Soft Matter**



PAPER View Article Online



Cite this: DOI: 10.1039/d0sm00384k

## Rheology of capillary foams†

Omotola Okesanjo, page Michael Tennenbaum, bc Alberto Fernandez-Nieves, bcd J. Carson Meredith xa and Sven H. Behrens xa

Aqueous foams are ubiquitous; they appear in products and processes that span the cosmetics, food, and energy industries. The versatile applicability of foams comes as a result of their intrinsic viscous and elastic properties; for example, foams are exploited as drilling fluids in enhanced oil recovery for their high viscosity. Recently, so-called capillary foams were discovered: a class of foams that have excellent stability under static conditions and whose flow properties have so far remained unexplored. The unique architecture of these foams, containing oil-coated bubbles and a gelled network of oil-bridged particles, is expected to affect foam rheology. In this work, we report the first set of rheological data on capillary foams. We study the viscoelastic properties of capillary foams by conducting oscillatory and steady shear tests. We compare our results on the rheological properties of capillary foams to those reported for other aqueous foams. We find that capillary foams, which have low gas volume fractions, exhibit long lasting rheological stability as well as a yielding behavior that is reminiscent of surfactant foams with high gas volume fractions.

## 1 Introduction

Received 3rd March 2020, Accepted 9th June 2020

DOI: 10.1039/d0sm00384k

rsc.li/soft-matter-journal

Aqueous foams are thermodynamically unstable systems consisting of a dispersion of gas bubbles in a continuous liquid. 1-3 Foams are thermodynamically unstable because the system free energy can be lowered by the loss of the air-water interfacial area. The structure of foams evolves over time due to the action of surface tension and Laplace pressure differences that minimize the gas-liquid interfacial area. Traditional aqueous foams are kinetically stabilized by surfactants or particles adsorbed at the gas-liquid interface. Surfactant molecules, when adsorbed at the air-water interface, keep the foam relatively stable by slowing down thinning and bursting of liquid films that separate bubbles, through steric or electrostatic repulsion, and through Marangoni flows that counteract surface tension gradients. 4,5 In the so called Pickering foams, particles adsorb at the air-water interface, forming a densely packed layer that limits coalescence.<sup>6-9</sup> Recently, a new class of long-term stable foams known as capillary foams (CFs) were discovered (see Fig. 1a). 10,111 CFs are made up of oil-coated bubbles that are enclosed within a gelled network

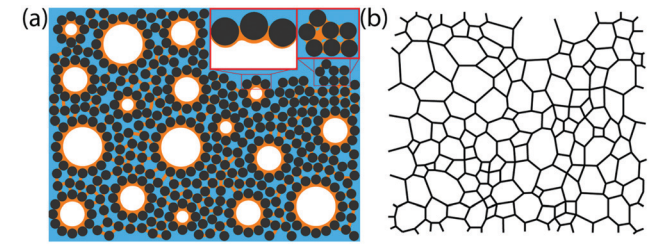


Fig. 1 (a) Schematic of capillary foam structure (bubble and particle sizes, and volume fractions are not to scale). (b) 2D representation of a high-quality surfactant foam (dry foam).

of oil-bridged particles (a capillary suspension).<sup>12</sup> The spherical bubbles in CFs are stabilized by the combined action of a small amount of a secondary immiscible liquid (the oil phase) and particles adsorbed at the oil-water interface.

Foams are widely applicable in a variety of products and processes across different industries because of their viscous and elastic properties. For instance, foams provide sensory benefits in foods and beverages like whipped cream, chocolate mousse, and beer.<sup>5</sup> Foams also find extensive applications in the cosmetics, pharmaceutical, material processing, and energy industries.<sup>4,13-17</sup> CFs, unlike surfactant foams, are oil resistant, long lasting and can be functionalized through oil-phase additives.<sup>11,18</sup> These additional and attractive properties of CFs open up opportunities for new foam applications in products and processes that are hindered by the above mentioned limitations of traditional foams. CFs, for example, could potentially be useful in enhanced oil recovery where oil-stable foams are

<sup>&</sup>lt;sup>a</sup> School of Chemical and Biomolecular Engineering, Georgia Institute of Technology, Atlanta, Georgia 30332, USA.

E-mail: carson.meredith@chbe.gatech.edu, sven.behrens@chbe.gatech.edu

<sup>&</sup>lt;sup>b</sup> School of Physics, Georgia Institute of Technology, Atlanta, Georgia 30332, USA

<sup>&</sup>lt;sup>c</sup> Department of Condensed Matter Physics, University of Barcelona, 08028 Barcelona. Spain

d ICREA-Institució Catalana de Recerca i Estudis Avançats, 08010 Barcelona, Spain
† Electronic supplementary information (ESI) available. See DOI: 10.1039/d0sm00384k

required to efficiently displace oil from underground reservoirs. However, to effectively apply CFs in these foam applications, a fundamental understanding of CF rheology is needed.4

The rheological properties of surfactant foams (SFs) have previously been studied for various foam applications. It has been shown that SFs with high gas volume fractions (= high "foam quality") behave either as solids or liquids depending on the applied stress. 19 When a small stress is applied to a foam, it deforms elastically like a solid. The rigidity of high quality foams comes from the tight packing of polyhedral bubbles within the foam matrix (see Fig. 1b). 13 Oscillatory rheology measurements show that the elastic modulus of SFs depends on the surface tension between the fluids and the mean bubble size. 20,21 These measurements also reveal a linear regime at low strain where both the storage and loss moduli are independent of the applied strain amplitude. At strains beyond the linear regime, the foam transitions from a solid-like to liquid-like response. This non-linear behavior is observed when the applied stress is strong enough to separate and rearrange neighboring bubbles.<sup>22,23</sup> In this case, the foam flows like a liquid as bubbles slide past each other.<sup>20,24</sup> When the applied stress is removed, the flow stops and the bubbles relax to a new configuration.<sup>25</sup> The observed elastic behavior disappears when the foam quality  $(\phi)$  falls below random close packing, which for spheres corresponds to  $\phi_{rcp} = 0.64^{26}$  At low foam quality ( $\phi < \phi_{rcp}$ ), SFs behave like a bubbly liquid as a result of the loose packing of spherical bubbles within the continuous phase.<sup>27</sup> Many of these rheological properties of SFs are similar to those observed in other soft dispersion systems, including concentrated emulsions, pastes, and dispersions of microgel beads. 19,28-30

With their oil-coated bubbles embedded in a particle network, 11 CFs are structurally distinct from the traditional aqueous foams described above, but somewhat similar to other soft materials: emulsions, capillary suspensions and colloidal gel foams. 12,31,32 The crucial differences between CFs and colloidal gel foams are that, in CFs, oil-mediated capillary forces provide the attractive particle-particle interactions and that the particles do not stabilize a gas-water interface, but rather the oil-water interface of oil-coated bubbles. Given the similarities and differences that CFs share with other dispersion and colloidal systems, one might speculate that CF rheology is governed by generic responses observed in these other soft dispersion systems.<sup>27</sup> However, the rheology of CFs has never been studied. The purpose of this work is thus to take a first look at CF rheology and how it deviates from the rheology of traditional surfactant and Pickering foams, as well as capillary suspensions.

In this paper, we present the first set of rheological data on capillary foams. We conduct oscillatory and steady shear experiments on a rheometer using parallel plate and Couette geometries. We then outline and discuss CF properties and we compare our observations to the rheological properties reported for traditional aqueous foams and other soft materials. Lastly, we discuss, the implications of these results in relation to potential applications of CFs in the tuning of processes and formulation of foam products.

## 2 Methods and materials

### 2.1 Capillary foam preparation

Polyvinyl chloride particles (PVC, Vinnolit SA1062/7, particle density: 1.41 g cm<sup>-3</sup>, average particle size 14.5 μm) were obtained from Vinnolit, Germany. 10 Trimethylolpropane trimethacrylate (TMPTMA) was obtained from Sigma-Aldrich. Deionized (DI) water with resistivity 18.2  $M\Omega$  cm was used as the aqueous phase. Foams were prepared using a rotor-stator homogenizer (IKA Ultra-Turrax T10, rotor diameter of 6.1 mm, stator diameter 8 mm).

Capillary foams were prepared by frothing a mixture of PVC particles (10 wt%), TMPTMA (2 wt%) and DI water (88 wt%). Two grams of PVC particles were first suspended in DI water and sonicated for 1 h (VWR, B2500A-MT). Once sonication was completed, TMPTMA was added to the suspension and the mixture was homogenized at 30 000 rpm for 3 min. We note that capillary foams of a similar composition were studied before, although not with regard to their rheological properties, and it was shown that in the absence of the oil component frothing does not lead to a stable foam, because the PVC particles used here are too hydrophilic to stabilize the air-water interface of a Pickering foam. 10

#### Rheology measurements

We use an Anton Paar MCR 501 parallel plate (PP) rheometer equipped with a temperature controller and evaporation blocker to perform rheological measurements on capillary foams. Shear localization and wall-slip of the foam within the confines of the measuring instrument are known to lead to inaccuracies in rheological measurements. <sup>13</sup> As such, the top plate (diameter of 40 mm) was lined with sandpaper (≅130 µm grain size, Porter Cable) to minimize slip in the measurements. A Couette geometry (bob length and diameter: 40 mm, 21 mm; cup diameter: 23 mm) was also used to obtain high shear rate data in controlled shear rate experiments. No sandpaper was used in the Couette bob or cup.

The prepared capillary foams were transferred carefully to the bottom plate (or Couette cup) of the rheometer. The gap height between the top and bottom plates was set to 4 mm, so that a substantial amount of foam could fit between the plates and account for the one-tenth rule of thumb for dispersed phases. 13 All measurements, unless stated otherwise, were obtained at this gap height. The temperature was maintained at 25 °C and the evaporation blocker was used to prevent drying of the foams. Once loaded, the CFs were allowed to equilibrate at rest for 20 min before the start of any steady or oscillatory shear experiments. Frequency sweep oscillatory measurements within the linear viscoelastic regime were obtained before and after each experiment to assess the state of the foam. Strain rates in the PP geometry vary across the plate or cup radius; we then report values of the apparent  $\dot{\gamma}$ . We replicate our data using fresh samples of CFs to ensure reproducibility.

## 3 Results and discussion

#### 3.1 Controlled stress and strain rate experiments

Capillary foams were subjected to controlled shear stress (CSS) and controlled strain rate (CSR) tests; both tests are steady

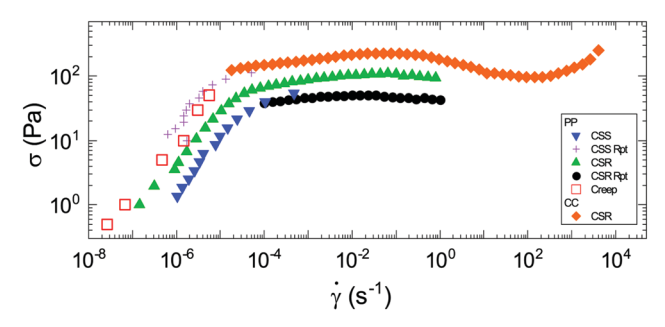


Fig. 2 Plot of stress versus strain rate of the CF; blue inverted triangles and violet cross (repeat) are obtained from controlled shear stress (CSS) experiments on a parallel plate (PP) setup; green triangles (PP), black circles (repeat on PP) and orange diamonds (Couette) are obtained from controlled strain rate (CSR) experiments; open red squares are obtained from creep experiments on PP

rotational tests in which the foam is either held at a specific stress or strain rate respectively. Fig. 2 shows the stress-strain rate curve (flow curve) from the CSS and CSR experiments; the differences between the curves are due to slight changes in gas volume fraction of the foam in the different experiments. The plot shows an initial increase in the stress with strain rate, followed by a stress plateau over a wide range of strain rates. At strain rates higher than those reported for the parallel-plate geometry, we observed that the CF was ejected from the gap between the rheometer plates. However, CSR experiments conducted in the Couette geometry, to obtain higher strain rate data on the CFs, show a later increase in stress; see orange diamond data at the highest strain rates.

From the flow curve in Fig. 2, we observe two different regimes where the stress  $(\sigma)$  increases with strain rate at low and high strain rates, and a third regime where the stress is not dependent on strain rate. Generally, for viscous liquids  $\sigma \propto \dot{\gamma}$ , while for elastic solids  $\sigma \propto \gamma$ , and  $\sigma \neq f(\dot{\gamma})$ .<sup>33</sup> The existence of these three regimes in the flow curve of CFs poses an important rheological question about the exact behavior of CFs; are CFs solid or are they a very viscous liquid? The key to this question resides in how to interpret the decrease in  $\sigma$  with decreasing  $\dot{\gamma}$ to the left of the stress-plateau as this can correspond to the aging of a solid foam, or to a final long-time relaxation of a very viscous foam. The flow curve itself is insufficient to answer this question. We thus perform oscillatory tests to characterize the elastic and viscous response of the foams and better understand their rheological properties.

#### 3.2 Strain amplitude sweeps

CFs were subjected to increasing strain amplitudes ( $\gamma$ ) at a constant frequency ( $\omega$ ) of 1 rad s<sup>-1</sup>. Fig. 3 shows the storage (G') and loss (G'') moduli of CFs and highlights the linear and nonlinear regimes of CFs within the range of the applied strain amplitudes  $(10^{-4} \text{ to } 10^{1})$ . The linear regime is the plateau region at low  $\gamma$ . For  $\gamma$  < 0.5, the CF is predominantly solid-like, with and elastic response (G') greater than the viscous response (G''). At a strain amplitude of 0.5, we observe a crossover between G' and G" indicating a transition from a solid-like to a liquid-like

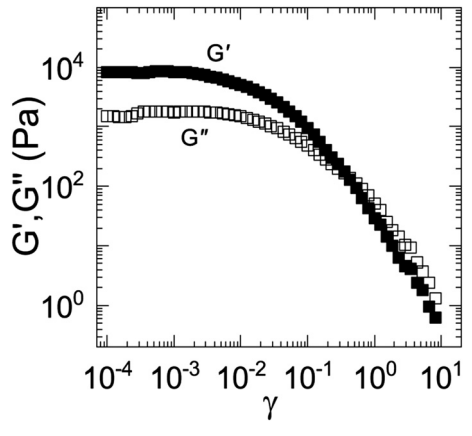


Fig. 3 Plot of G' (filled square) and G'' (open square) versus the applied strain amplitude at  $\omega = 1 \text{ rad s}^{-1}$ .

response. Above strains of 0.5, G'' is greater than G', indicating that the foam is fluidized and that the bubbles and capillary network are significantly strained and forced to rearrange. We also observed that the normal force on the top plate of the instrument gradually decreases during the strain sweep (Fig. S1, ESI†). The normal force does not recover when the strain sweep is repeated, reflecting a large strain induced structural rearrangement. The decreasing normal force is most likely due to bubble collapse, or to ejection of the CF from between the plates during fluidization.

The origin of the elastic properties observed in CFs, can be compared to those of SFs. CFs at 10 wt% particle and 2 wt% oil concentrations have an average foam quality of 32% (Fig. S2, ESI†), which corresponds to half the gas volume fraction where solid-like foam behavior is usually first observed in SFs. At the present foam quality, typical SFs are considered bubbly liquids containing loosely packed spherical bubbles. Rheology experiments show that low-quality SFs have no elasticity.<sup>26</sup> Although CFs may be classified as low-quality foams, their rheology shows a remarkably high elastic response comparable to that of high-quality SFs. Such strong elasticity is also observed in low quality colloidal gel foams, whose rheology one might expect to be similar to that of CFs.31 Given that the gelled particle network occupies as high as 70 vol% of the CF matrix, the elasticity of CFs is likely a result of the strong particle network that both encloses the bubbles and percolates the space between bubbles. For SFs, the elastic shear modulus is  $G_0 \sim \sigma/R$ , with  $\sigma$  the surface tension between the fluids and R the mean bubble radius.  $^{34}$  In contrast, for CFs,  $G_0$  is likely to depend on the concentration of particles in the foam, the strength of the capillary bridges in the particle network and the surface energy of the dual fluid interfaces (air-oil and particle laden oil-water) of the bubbles present in the foam. The concentration of the particles and the strength of the capillary bridges have previously been shown to influence the strength of capillary suspensions, the particle network component of CFs.<sup>35</sup>

The nonlinear response in the strain sweep also highlights another key difference between CFs and SFs. As the applied strain increases, CFs and SFs respond differently in the Paper Soft Matter

transition region. In SFs, G'' increases within the transition region as a result of Marangoni flows between stretched and compressed bubbles.  $^{20,36}$  An increase in G'' is not observed in CFs, suggesting that the rigid particle network structure, stabilized by the capillary bridges between the particles, prevents bubble deformation in the transition region. In fact, this behavior is observed in Pickering foam systems with significant steric barriers that prevent immediate destruction of bubbles. 36,37 In these systems, it was found that while bubble deformation occurs as both moduli decrease, bubble motion does not occur until the crossover between G' and G'' is reached.

Although the results of the strain sweep experiment on CFs show that G' > G'' in the linear "equilibrium" regime at low strain amplitudes and  $\omega = 1$  rad s<sup>-1</sup>, many viscoelastic materials show a frequency dependence. We then study the rheological response of CFs with respect to time and frequency.

#### 3.3 Time and frequency sweeps

The equilibrium structure and time-dependent response of CFs were probed in both time and frequency sweep experiments by applying an oscillatory strain within the linear regime ( $\gamma$  = 0.001). We monitored the storage and loss moduli of the CF at 10 rad s<sup>-1</sup> for 48 h in a time sweep experiment. Fig. 4a shows the long-time sweep experiment on the CF. The time sweep experiment shows that both elastic and viscous moduli of the

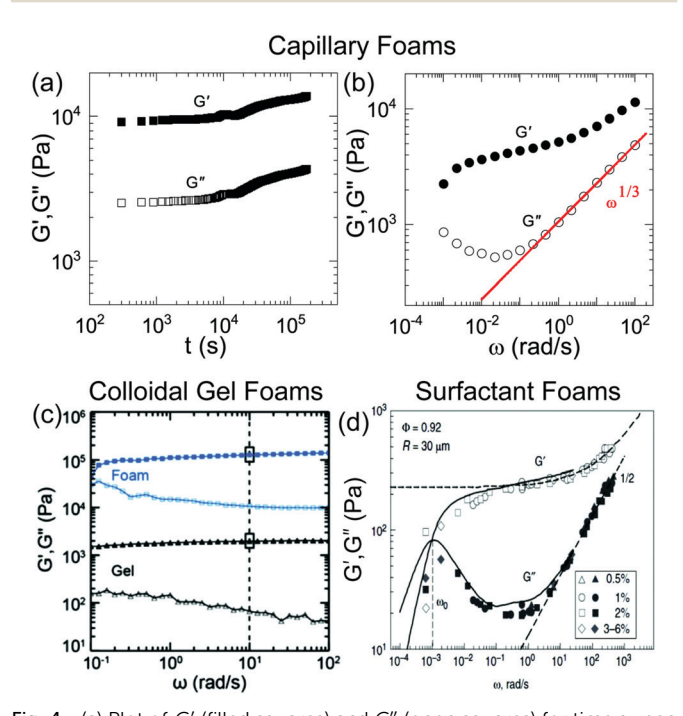


Fig. 4 (a) Plot of G' (filled squares) and G'' (open squares) for time sweep measurement at  $\omega = 10 \text{ rad s}^{-1}$  on the CFs. (b) Plot of G' (filled circles) and G'' (open circles) for a frequency sweep at  $\gamma = 0.001$  on CFs. (c) Plot of G'(filled symbols) and G'' (open symbols) for a frequency sweep on colloidal gels and gel foams (adapted with permission from ref. 32. Copyright 2017 American Chemical Society). (d) Plot of G' (open symbols) and G'' (filled symbols) for a frequency sweep on surfactant foams; symbols denote the imposed strain amplitude (adapted from ref. 39. Reprinted with permission from ref. 16).

CFs are stable over the course of two days; G' and G'' are essentially constant up to  $2 \times 10^4$  s and only slightly increase afterwards. In the architecture of CFs, bubbles are not only connected in a space-spanning particle network but are also enclosed by two fluid-fluid interfaces (oil-air and oil-water). The effects of bubble and particle network connectivity and dual fluid interfaces produce long term foam stability that allows for persistence of the foam rheological response over time. This long-term stability is remarkable given that the continuous evolution of foam structure typically limits the experimentation time in foam rheology measurements. This type of rheological stability is not common among SFs because they tend to be subject to more rapid bubble coalescence and collapse. It is worth mentioning that Pickering foams and colloidal gel foams are perhaps the only other type of aqueous foams that may be capable of similar stability because of the presence of a particle network or particle packing that kinetically stabilizes the fluid interface. 1,31

The frequency sweep plot in Fig. 4b shows both the viscous and the elastic response of the CFs over a wide range of frequencies. A stronger elastic response is observed at all frequencies probed; however, G' is observed to increase monotonically. When the foam is probed from high to low frequencies, G'' decreases, exhibits a minimum and subsequently increases again. We believe that the increase in G'' and decrease in G' toward low frequencies is a result of bubble coalescence and particle network rearrangements within the CF matrix. The frequency sweep data for both CFs and high quality SFs highlights the kinetic changes that occurs in both foam types, showing that aging can lead to structural rearrangements that cause G' < G'' over long periods of time.<sup>38</sup> Although the elasticity of CFs arises from the particle network in their gel matrix, their frequency dependent behavior is qualitatively similar to that of particle-free SFs (Fig. 4b and d). Although  $G'' \sim \omega^{1/3}$  in our CF at high frequencies, in contrast to the  $\omega^{1/2}$ dependence reported for SFs,27 the moduli obtained from the frequency sweep experiments suggest that CFs are more similar to SFs than to colloidal gel (Pickering) foams (Fig. 4c) in their frequency dependent behavior. 31 Note, however the differences in the values of the moduli: both the G' and G'' values of CFs are significantly larger than those of typical SFs.

The qualitative similarity of capillary foams and surfactant foams in the frequency sweeps suggests that in both systems it is the bubble network that determines the overall flow behavior, despite the fact that the mechanical coupling between bubble deformations occurs through the particle network in CFs and through direct contact in SFs. The weaker frequency dependence of G'' (lower exponent) at high frequencies in CFs indicates a less pronounced dissipation in this regime, which could result from the presence of rigid structures. This is consistent with the observed lower frequency dependence  $(G'' \sim \omega^{\nu})$  with  $\nu < 1/2$  in SFs with high interfacial rigidity due to the presence of co-surfactants with low water solubility.<sup>39</sup> In CFs bubble rigidity stems from the bubbles' composite coat of oil and particles and its coupling to a stiff network of oil-bridged particles that further contributes to

diminishing dissipation and thereby shifting the short time relaxation ("beta relaxation") to higher frequencies (shorter time scales).

Above all the oscillatory tests show that the unique structure of CFs leads to distinct foam rheology that sets these foams apart both from previously studied colloidal gel foams, and from traditional surfactant stabilized foams. The frequency sweep also helps determine the characteristic relaxation time  $(\tau_c)$  of the CFs corresponding to the crossover of G' and G'' at low  $\omega$ .<sup>33</sup> We determine  $\tau_c$  from the crossover frequency  $\omega_c$ :

$$\tau_{\rm c} = \frac{2\pi}{\omega_{\rm c}} \tag{1}$$

By extrapolating the data in Fig. 4b to lower frequencies, we expect that G' and G'' will intersect at  $10^{-4} < \omega_c < 5 \times 10^{-4}$  rad  $\rm s^{-1}$ . The relatively long characteristic time (  $\sim 10^4$  s) observed in CFs is similar to the characteristic time of SFs.<sup>38</sup> However, while the slow linear viscoelastic response in SFs results from coarsening of the foam and Marangoni flows in the foam's liquid films, the timescale of the slow viscoelastic response of CFs is dictated by particle network rearrangements over time. CF rheology suggests that G' < G'' at low frequencies because aging unjams the CFs over time. The onset of this long-time viscous dominance occurs on timescale on the order of  $\tau_c$ .

#### 3.4 Stress relaxation

To further study the rheological behavior of the CFs, we perform stress relaxation experiments and apply a constant strain to the foam while monitoring the time dependence of the stress. 40 Fig. 5 shows the result of stress relaxation experiments performed on CFs. The unperturbed response of the CF corresponds to the blue curve, where a strain of zero ( $\gamma \ll 10^{-6}$ ), within the limits of the rheometer, is applied.

For a strain of  $\gamma = 0.005$  within the linear regime (see Fig. 3), we observe in Fig. 5 that the stress on the foam significantly relaxes after  $\sim 6$  h (22 000 s); the relaxation time, obtained by fitting the long-time stress decay to an exponential function, is  $4.6 \times 10^4$  s and thus comparable to the  $\tau_c$  obtained from the frequency sweep experiment. The relaxation behavior observed in CFs is typical of viscoelastic materials and confirms that

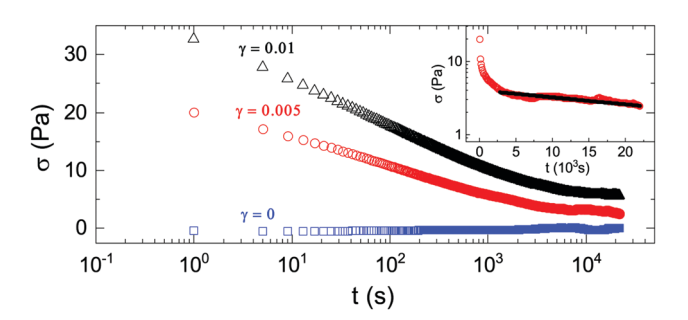


Fig. 5 Plot of stress versus time on CFs during stress relaxation experiments. Symbols correspond to applied strains below  $10^{-6}$  (blue squares), applied strain in the linear regime at  $\gamma = 0.005$  (red circles), and applied strain outside the linear regime at  $\gamma = 0.01$  (black triangles). The black line in the inset shows an exponential fit to the stress curve for  $\gamma = 0.005$ .

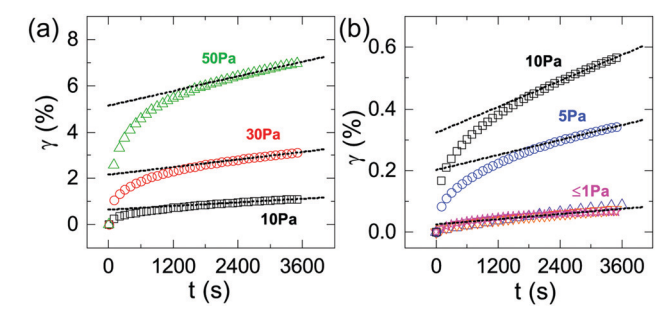


Fig. 6 Plot of strain versus time in creep experiments; (a) with applied stresses at 50 Pa (green triangles), 30 Pa (red circles), and 10 Pa (black squares). (b) Plots of lower stresses at 10 Pa (black squares), 5 Pa (blue circles), 1 Pa (pink stars), 0.5 Pa (orange inverted triangles) and 0 Pa (violet triangles). Black dashed lines show linear fits used to obtain  $\dot{\gamma}$ .

 $\tau_{\rm c}$  predicted by the frequency sweep is indeed a result of relaxation processes. Note that for a strain of  $\gamma = 0.01$  which is outside the linear regime (see Fig. 3), the stress on the foam never recovers during the experimental time, indicating that plastic deformation has occurred.

## 3.5 Creep experiments

Creep experiments were performed to study in detail the longtime behavior of the CFs under stress. In these experiments, we applied a constant stress and measured the time dependence of the strain. Fig. 6 shows the strain response at applied stresses  $(\sigma)$  ranging from 0.5 Pa to 50 Pa. All plots show a general trend of three strain regimes that include an initial fast strain increase, a transition zone and a linearly increasing strain.

The fast initial strain increase corresponds to the short-time elastic response of the material to the applied  $\sigma$  while the linear increase in strain is indicative of a long-time viscous behavior. From the linear fits in this region, we obtain  $\dot{\gamma}$ . By further using the value of the applied stress, we obtain the viscosity.

$$\eta = \frac{\sigma}{\dot{\gamma}} \tag{2}$$

The result of the creep experiments indicate that CFs exhibit viscous flow over long time periods even for minute applied stresses. When an infinitesimal stress ( $\sigma = 0$  Pa) is applied to the CFs, the instrument measures a strain increase over the experimental time (see violet triangles in Fig. 6b). We note that this strain increase, which is on the order of 10<sup>-4</sup>, is within the detection limits of the instrument, which is  $\gamma \geq 10^{-6}$ , and is taken to be the strain increase of the unperturbed CF. We believe that this minute strain increase is caused by coarsening and particle network restructuring that results from the nonequilibrium nature of foams as seen in the frequency sweep experiments. When  $\sigma = 0.5$  Pa or 1 Pa, the strain increase measured is similar to that obtained when  $\sigma = 0$  Pa. However, for  $\sigma > 5$  Pa, the strain increases by at least an order of magnitude. From Fig. 7 however, we observe a continuous decrease in  $\dot{\gamma}$  over time, showing that the strain increase induced by the applied stresses results in a non-steady-state flow of the CF. The higher stresses applied (10, 30, 50 Pa) apparently

Paper Soft Matter

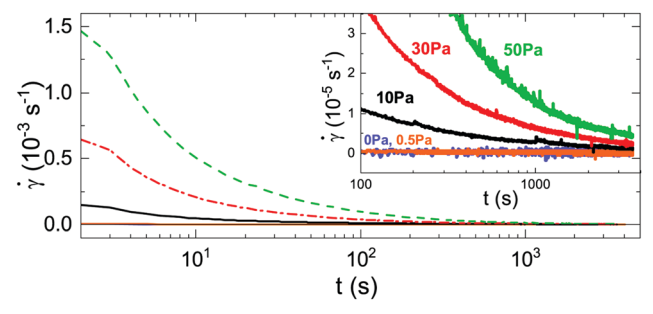


Fig. 7 Evolution of strain rate in capillary foams during creep experiments; magnification of strain rate *versus* time at longer time periods (inset). Applied stresses at 50 Pa (green dashes), 30 Pa (red dash dots), 10 Pa (black line), 0.5 Pa (orange line) and 0 Pa (violet line).

lead to an increased initial rate of structural rearrangements in the foam, but eventually the induced strain rates still decay to the level observed even in the absence of any significant externally applied stress.

To further elaborate on this, using the viscosity ( $10^7$  Pa s) obtained from the creep experiments and the plateau modulus ( $G_p = 10^3$  Pa) of G' in the frequency sweep (see Fig. 4b), we divide them both to obtain a time scale,

$$\tau = \frac{\eta_{\text{creep}}}{G_{\text{p}}} \tag{3}$$

which is on the order of  $\tau_c$ , suggesting that the viscous behavior observed in the creep experiments (Fig. 6) is actually related to aging events resulting from rearrangements in the foam.

The combined results of the oscillatory, stress relaxation and creep experiments help understand the flow curve of CFs (see Fig. 2). From the oscillatory and stress relaxation experiments, we find that the CF is a solid undergoing aging on a timescale of  $\tau_c \approxeq 10^4$  s. From the creep experiments, we observe that stresses  $\le 50$  Pa cause small deformation rates ( $\dot{\gamma} \ll 1/\tau_c$ ), indicative of particle network rearrangements. These results confirm that the CF flow curve is representative of a solid undergoing aging that yields at sufficiently large stresses.

The CF flow curve is also quite similar to the flow curves of Gillette shaving foams, mayonnaise emulsions and polystyrene suspensions obtained by Da Cruz et al.28 The authors in that study also attribute the initial stress increase regime to structural rearrangements within the foam. This explanation is consistent with the results of our creep experiments on CFs, which show that for a given range of applied stresses, decreasing strain rates are observed as the CF relaxes to new configurations. Further work done by Coussot et al. also shows that the plateau in the stress results from the acceleration and deceleration of  $\dot{\gamma}$ at certain stresses.41 They observed, going from low to high stresses, that below a critical stress value ( $\sigma_{c1}$ ),  $\dot{\gamma}$  continuously decreases with time and that beyond a second critical stress value ( $\sigma_{c2}$ ),  $\dot{\gamma}$  accelerates to a constant value. At intermediate stresses (between both critical stress values),  $\dot{\gamma}$  first increases and then rapidly falls off. 42 While we certainly observed that  $\dot{\gamma}$ continuously decreases below 70 Pa  $< \sigma_{c1} < 100$  Pa, we could not reach values above the second critical stress ( $\sigma_{c2}$ ) before the CFs are ejected from between the gap of the rheometer plates. Data on the CFs could not be gathered beyond a stress of 128 Pa using the parallel plate geometry.

The point at which the stress plateau occurs is said to closely correspond to the value of the yield stress of the material when an increasing stress protocol is used. Flow curves of yield stress materials show that the stress tends to a finite value as the strain rate approaches zero. For example, the reported flow curve of carbopol microgels, shows a yield stress on the order of tens of Pascal at a strain rate of  $10^{-3}$  s $^{-1}$ . From the results of our CSS and CSR experiments, we estimate that the value of the yield stress of the CFs is about 100 Pa. The yield stress value obtained for CFs is very similar to that of CGFs, which have  $\sigma_{\rm y} \sim 110$  Pa, showing again that CFs are highly elastic materials.

While there are disputes concerning the existence of a yield stress in soft materials, 45-47 the notion of a yield stress and the transition from solid-like to fluid-like behavior in foams have been justified by the observations of Lissajous curves and strain sweeps in oscillatory experiments, start-up shear experiments and flow curves of CSS. 24,48,49 Although we observe a similar trend in the strain sweeps of CFs, where the loss and storage moduli cross over in the strain sweep plot, sample ejection in parallel plate and slip limitations in (see Fig. S3, ESI†) Couette geometry prevented us from obtaining the full flow curve of the CFs from CSS experiments. Slip is an experimental artifact that can lead to errors in yield stress determination. 50 Although most of the data presented in this work were obtained using roughened plates, it is possible that our data is influenced by slip. Marze et al. for instance, observed slip contributions to their foam rheology data despite using rough shearing surfaces; they commented that slip existence is dependent on both the applied shear rate and plate roughness.<sup>51</sup> When smooth shearing surfaces are used, as is the case in our Couette experiments, three different slip regimes are observed. Meeker et al. observed that for  $\sigma \ll \sigma_{\rm v}$ , motion is due to wall slip, for  $\sigma \approx \sigma_{\rm v}$ , motion is due to both slip and yielding contributions, and for  $\sigma \gg \sigma_{\rm v}$  slip is negligible.<sup>30,52</sup> The decrease in stress observed at  $0.1 < \dot{\gamma} < 100 \, \rm s^{-1}$  during the CSR experiment in the Couette geometry (orange diamond plot in Fig. 2) could then reflect the stress-induced structural rearrangement prior to yielding and the possible influence of slip. At lower  $\dot{\gamma}$ , the accurate determination of the yield stress of CFs requires the careful study of the exact nature and extent of slip in our experiments; this could be done using microscopic techniques.<sup>50</sup> Alternately, a vane geometry, which has been shown to effectively suppress slip effects in structured fluids, can also be used to increase the accuracy of the yield stress determination.53 The yield stress determined in our experiments should only be taken as a rough first estimate.

The yield stress in our CFs is lower than the yield stress (of  $\sim$  400 Pa) inferred from measurements on the capillary suspensions that form the continuous phase of our CFs (see Fig. S4, ESI†), and lower also than values reported previously for other capillary suspensions ( $\sigma_{\rm y,cs} \sim 300$ –10 000 Pa),  $^{12,54,55}$  but falls within the range of the yield stresses reported for some SFs and Pickering foams ( $\sigma_{\rm y,foam} \sim 20$ –200 Pa).  $^{28,36,48}$  Although the yield stress in suspensions and foams is typically governed by the

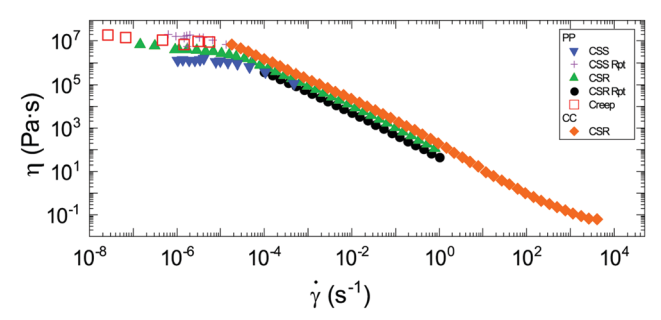


Fig. 8 Viscosity versus strain rate plot corresponding to the flow curve in Fig. 2. Blue inverted triangles and violet cross (repeat) are obtained from controlled shear stress (CSS) experiments on a parallel plate (PP) setup; green triangles (PP), black circles (repeat on PP) and orange diamonds (Couette) are obtained from controlled strain rate (CSR) experiments; open red squares are obtained from creep experiments on PP

volume fraction of a single dispersed phase, the notion of yielding as the result of dispersed moieties unjamming still likely applies in those materials and CFs alike. 1,16,27,35

Lastly, in Fig. 8, we plot the viscosity of the CFs as a function of the strain rate. The plot shows that CFs shear thin after they yield. At low strain rates, the CFs behave 'extremely viscous', having viscosities 10<sup>10</sup> times the viscosity of water. As seen from the creep experiments, the viscosity at  $\dot{\gamma} \leq 10^{-5} \, \mathrm{s}^{-1}$  result from the restructuring (aging) of CFs and are non-steady state viscosities. At higher  $\dot{\gamma}$ , the viscosity decreases with increasing strain rate with a slope of -1, corresponding to the plateau region of the flow curve. CSR experiments show that the shear thinning behavior of CFs at high strain rates is similar to that of surfactant foams described in the literature. 3,48,56 Even at the highest strain rates observed, the viscosity of our CFs remains significantly higher than the viscosity of water.

The rheological data presented in this work characterizes CFs as an aging solid because of their out-of-equilibrium nature. The behavior observed in CFs is similar to that of crystalline solids like ice that are known to flow at long time scales.<sup>57</sup> While the apparent fluid nature in crystalline solids is defect mediated, the non-equilibrium nature in foams results in the observed aging. Aging has also been observed in similar out-of-equilibrium soft materials like emulsions and microgels. 58,59 The aging dynamics of CFs, though beyond the scope of this work, resembles the glassy dynamics of disordered hard materials and might be understood using models of soft glassy rheology.<sup>60</sup>

## 4 Conclusions

We have investigated the rheological properties of capillary foams by carrying out oscillatory and steady shear rotational measurements. Reproducible measurements of this kind are greatly facilitated by the excellent long-term stability of capillary foams. Our results show that capillary foams (CFs), despite their low gas volume fraction (low "foam quality"), are rheologically quite similar to high quality surfactant foams. Oscillatory measurements on the CFs at a frequency of 1 rad s<sup>-1</sup> reveal the dominance of elastic behavior over viscous behavior,

which is not known from low quality surfactant foams but has been observed in low quality colloidal gel (Pickering) foams, albeit with a very different frequency dependence of the viscoelastic moduli than reported here for CFs. Time sweep experiments lasting 48 h show consistent elastic and viscous responses of CFs with slight increases of both moduli after 10<sup>4</sup> s. The strong elastic properties and long term stability observed in CFs are results of the oil-stabilized particle network and particle-stabilized oil coat surrounding the bubbles. Frequency sweeps and stress relaxation measurements indicate that the characteristic relaxation time of CFs is on the order of 104 s and that CFs exhibit plastic deformation when subjected to high strains. Creep experiments on CFs show short time elastic response and foam restructuring over long time periods. Results from creep, controlled stress and strain rate experiments are all consistent with a yield stress in CFs on the order of 100 Pa and a long-time aging behavior. Controlled strain rate measurements also show that CFs possess high viscosities and are shear thinning after yielding in the non-linear regime. The high viscosity observed here, in conjunction with the known CF stability against contact with an oil phase, suggests that CFs could be useful as displacing fluids in enhanced oil recovery. We believe that the unique structure and composition of capillary foams and their resulting rheological properties offer further opportunities for foam related innovations ranging from low fat foods to novel foam formulations for health care, cosmetics, and household products. More detailed studies will obviously be required to enable the requisite engineering of foam rheology.

## Conflicts of interest

The authors declare no conflict of interest.

# Acknowledgements

The work in this paper was made possible with the financial support from the National Science Foundation (CBET-1706475; DMR-1609841) and MCIU/AEI/FEDER, UE (Grant No. PGC2018-336 097842-B-I00). We would also like to acknowledge the generous donation of PVC particles from Vinnolit (Germany).

## References

- 1 E. Blanco, S. Lam, S. K. Smoukov, K. P. Velikov, S. A. Khan and O. D. Velev, Langmuir, 2013, 29, 10019-10027.
- 2 U. T. Gonzenbach, A. R. Studart, E. Tervoort and L. J. Gauckler, Angew. Chem., Int. Ed., 2006, 45, 3526-3530.
- 3 T. Firoze Akhtar, R. Ahmed, R. Elgaddafi, S. Shah and M. Amani, J. Pet. Sci. Eng., 2018, 162, 214-224.
- 4 D. T. Wasan and S. P. Christiano, Handbook of Surface and Colloid Chemistry, ed. K. S. Birdi, CRC Press, 1997, ch. 6, pp. 180-215.
- 5 D. L. Weaire and S. Hutzler, The Physics of Foams, Clarendon Press, 2001.

- 6 W. Ramsden and F. Gotch, Proc. R. Soc. London, 1904, 72, 156–164.
- 7 S. U. Pickering, J. Chem. Soc., Trans., 1907, 91, 2001-2021.
- 8 B. P. Binks, Curr. Opin. Colloid Interface Sci., 2002, 21-41.
- R. Aveyard, B. P. Binks and J. H. Clint, Adv. Colloid Interface Sci., 2003, 100–102, 503–546.
- 10 Y. Zhang, J. Wu, H. Wang, J. C. Meredith and S. H. Behrens, Angew. Chem., Int. Ed., 2014, 53, 13385–13389.
- 11 Y. Zhang, S. Wang, J. Zhou, G. Benz, S. Tcheimou, R. Zhao, S. H. Behrens and J. C. Meredith, *Ind. Eng. Chem. Res.*, 2017, 56, 9533–9540.
- 12 E. Koos and N. Willenbacher, Science, 2011, 331, 897.
- 13 Foams: theory, measurement and applications, ed. S. A. Khan and R. K. Prud'homme, 1995.
- 14 B. E. Chavez-Montes, L. Choplin and E. Schaer, *J. Texture Stud.*, 2007, **38**, 236–252.
- 15 E. Dickinson, Curr. Opin. Colloid Interface Sci., 2010, 15, 40-49.
- 16 Foam Engineering: Fundamentals and Applications, ed. P. Stevenson, John Wiley & Sons, 2012.
- 17 B. P. Binks, K. Muijlwijk, H. Koman and A. T. Poortinga, *Food Hydrocolloids*, 2017, **63**, 585–592.
- 18 Y. Zhang, M. C. Allen, R. Zhao, D. D. Deheyn, S. H. Behrens and J. C. Meredith, *Langmuir*, 2015, **31**, 2669–2676.
- 19 H. M. Princen and A. D. Kiss, J. Colloid Interface Sci., 1986, 112, 427–437.
- 20 S. Marze, R. M. Guillermic and A. Saint-Jalmes, *Soft Matter*, 2009, 5, 1937–1946.
- 21 T. G. Mason and D. A. Weitz, *Phys. Rev. Lett.*, 1995, 74, 1250–1253.
- 22 M. Durand and H. A. Stone, Phys. Rev. Lett., 2006, 97, 226101.
- 23 A.-L. Biance, S. Cohen-Addad and R. Höhler, *Soft Matter*, 2009, 5, 4672–4679.
- 24 F. Rouyer, S. Cohen-Addad, R. Höhler, P. Sollich and S. M. Fielding, *Eur. Phys. J. E: Soft Matter Biol. Phys.*, 2008, 27, 309–321.
- 25 S. Cohen-Addad, R. Höhler and O. Pitois, *Annu. Rev. Fluid Mech.*, 2013, 45, 241–267.
- 26 A. Saint-Jalmes and D. J. Durian, *J. Rheol.*, 1999, **43**, 1411–1422.
- 27 R. Höhler and S. Cohen-Addad, *J. Phys.: Condens. Matter*, 2005, **17**, R1041–R1069.
- 28 F. Da Cruz, F. Chevoir, D. Bonn and P. Coussot, *Phys. Rev. E: Stat., Nonlinear, Soft Matter Phys.*, 2002, **66**, 051305.
- 29 P. Hébraud, F. Lequeux and J. F. Palierne, *Langmuir*, 2000, 16, 8296–8299.
- 30 S. P. Meeker, R. T. Bonnecaze and M. Cloitre, J. Rheol., 2004, 48, 1295–1320.
- 31 J. T. Muth and J. A. Lewis, Langmuir, 2017, 33, 6869-6877.
- 32 E. Koos and N. Willenbacher, *Soft Matter*, 2012, **8**, 3988–3994.
- 33 R. G. Larson, *The Structure and Rheology of Complex Fluids*, OUP, USA, 1999.

- 34 A. M. Kraynik, D. A. Reinelt and F. van Swol, *Phys. Rev. Lett.*, 2004, **93**, 208301.
- 35 E. Koos, J. Johannsmeier, L. Schwebler and N. Willenbacher, Soft Matter, 2012, 8, 6620–6628.
- 36 M. Lexis and N. Willenbacher, *Colloids Surf.*, A, 2014, 459, 177–185.
- 37 M. Hermes and P. S. Clegg, Soft Matter, 2013, 9, 7568-7575.
- 38 A. D. Gopal and D. J. Durian, *Phys. Rev. Lett.*, 2003, **91**, 188303.
- 39 S. Costa, R. Höhler and S. Cohen-Addad, *Soft Matter*, 2013, 9, 1100–1112.
- 40 H. M. Wyss, in *Fluids, Colloids and Soft Materials: An Introduction to Soft Matter Physics*, ed. A. Fernandez-Nieves and A. M. Puertas, Wiley, 2016.
- 41 P. Coussot, Rheometry of Pastes, Suspensions and Granular Materials: Applications in Industry, John Wiley & Sons, 2005.
- 42 P. Coussot, Q. D. Nguyen, H. T. Huynh and D. Bonn, J. Rheol., 2002, **46**, 573–589.
- 43 P. Moller, A. Fall, V. Chikkadi, D. Derks and D. Bonn, *Philos. Trans. R. Soc.*, *A*, 2009, **367**, 5139–5155.
- 44 C. J. Dimitriou, R. H. Ewoldt and G. H. McKinley, *J. Rheol.*, 2013, **57**, 27–70.
- 45 D. Bonn, M. M. Denn, L. Berthier, T. Divoux and S. Manneville, *Rev. Mod. Phys.*, 2017, **89**, 035005.
- 46 F. Rouyer, S. Cohen-Addad and R. Höhler, *Colloids Surf., A*, 2005, **263**, 111–116.
- 47 A. Ö. Özarmut and H. Steeb, *J. Phys.: Conf. Ser.*, 2015, **602**, 012031.
- 48 S. A. Khan, C. A. Schnepper and R. C. Armstrong, *J. Rheol.*, 1988, **32**, 69–92.
- 49 B. Herzhaft, S. Kakadjian and M. Moan, *Colloids Surf.*, A, 2005, **263**, 153–164.
- 50 M. Cloitre and R. T. Bonnecaze, Rheol. Acta, 2017, 56, 283-305.
- 51 S. Marze, D. Langevin and A. Saint-Jalmes, *J. Rheol.*, 2008, 52, 1091–1111.
- 52 S. P. Meeker, R. T. Bonnecaze and M. Cloitre, *Phys. Rev. Lett.*, 2004, **92**, 198302.
- 53 N. Q. Dzuy and D. V. Boger, J. Rheol., 1985, 29, 335-347.
- 54 E. Koos, W. Kannowade and N. Willenbacher, *Rheol. Acta*, 2014, 53, 947–957.
- 55 K. D. Danov, M. T. Georgiev, P. A. Kralchevsky, G. M. Radulova, T. D. Gurkov, S. D. Stoyanov and E. G. Pelan, *Adv. Colloid Interface Sci.*, 2018, 251, 80–96.
- 56 B. Herzhaft, Oil Gas Sci. Technol., 1999, 54, 587-596.
- 57 W. B. Durham, O. Prieto-Ballesteros, D. L. Goldsby and J. S. Kargel, *Space Sci. Rev.*, 2010, **153**, 273–298.
- 58 M. Cloitre, R. Borrega and L. Leibler, *Phys. Rev. Lett.*, 2000, **85**, 4819–4822.
- 59 L. Cipelletti, L. Ramos, S. Manley, E. Pitard, D. A. Weitz, E. E. Pashkovski and M. Johansson, *Faraday Discuss.*, 2003, 123, 237–251.
- 60 R. Bandyopadhyay, D. Liang, J. L. Harden and R. L. Leheny, *Solid State Commun.*, 2006, **139**, 589–598.